GROUND-BASED RADIOMETRIC MEASUREMENTS OF SLANT PATH ATTENUATION IN THE V/W BANDS

APRIL 2016

FINAL TECHNICAL REPORT

APPROVED FOR PUBLIC RELEASE; DISTRIBUTION UNLIMITED

STINFO COPY

AIR FORCE RESEARCH LABORATORY
INFORMATION DIRECTORATE

■ **AIR FORCE MATERIEL COMMAND**   ■   **UNITED STATES AIR FORCE**   ■   **ROME, NY 13441**

NOTICE AND SIGNATURE PAGE

AFRL-RI-RS-TR-2016-100   HAS BEEN REVIEWED AND IS APPROVED FOR PUBLICATION IN ACCORDANCE WITH ASSIGNED DISTRIBUTION STATEMENT.

FOR THE CHIEF ENGINEER:

/ S /
RICHARD MICHALAK
Chief, Information Transmission Branch
Computing & Communications Division

/ S /
JOESEPH A. CAROLI
Acting Technical Advisor
Computing & Communications Division
Information Directorate

REPORT DOCUMENTATION PAGE

Form Approved
OMB No. 0704-0188

1. REPORT DATE (DD-MM-YYYY)	2. REPORT TYPE	3. DATES COVERED (From - To)
APR 2016	FINAL TECHNICAL REPORT	OCT 2012 – SEP 2015

4. TITLE AND SUBTITLE

GROUND-BASED RADIOMETRIC MEASUREMENTS OF
SLANT PATH ATTENUATION IN THE V/W BANDS

5a. CONTRACT NUMBER
IN-HOUSE (R0YD)

5b. GRANT NUMBER
N/A

5c. PROGRAM ELEMENT NUMBER

6. AUTHOR(S)

George Brost; Kevin Magde

5d. PROJECT NUMBER
T2WB

5e. TASK NUMBER
IN

5f. WORK UNIT NUMBER
HO

7. PERFORMING ORGANIZATION NAME(S) AND ADDRESS(ES)
Air Force Research Laboratory/Information Directorate
Rome Research Site/RITE
525 Brooks Road
Rome NY 13441-4505

8. PERFORMING ORGANIZATION REPORT NUMBER

N/A

9. SPONSORING/MONITORING AGENCY NAME(S) AND ADDRESS(ES)
Air Force Research Laboratory/Information Directorate
Rome Research Site/RITE
525 Brooks Road
Rome NY 13441-4505

10. SPONSOR/MONITOR'S ACRONYM(S)
AFRL/RI

11. SPONSORING/MONITORING AGENCY REPORT NUMBER
AFRL-RI-RS-TR-2016-100

12. DISTRIBUTION AVAILABILITY STATEMENT
Approved for Public Release; Distribution Unlimited. PA# 88ABW-2016-1702
Date Cleared: 31 MAR 16

13. SUPPLEMENTARY NOTES

14. ABSTRACT

Ground-based radiometric techniques were applied to measure the slant path attenuation cumulative distribution function to over 20 dB of attenuation and to less than 1% exceedance probability at the V and W band frequencies of 72.5 and 82.5 GHz. A model based approach was used to invert brightness temperature to attenuation. An atmospheric model relevant to the geographic location and statistically representative of the attenuating conditions was developed for this purpose. Monte-Carlo solutions to the radiative transfer equation for the precipitating atmosphere were used to generate the attenuation retrieval algorithm.

15. SUBJECT TERMS

Radio wave propagation, remote sensing, instruments and techniques

16. SECURITY CLASSIFICATION OF:			17. LIMITATION OF ABSTRACT	18. NUMBER OF PAGES	19a. NAME OF RESPONSIBLE PERSON KEVIN MAGDE
a. REPORT U	b. ABSTRACT U	c. THIS PAGE U	UU	39	19b. TELEPHONE NUMBER (Include area code) N/A

Standard Form 298 (Rev. 8-98)
Prescribed by ANSI Std. Z39.18

CONTENTS

FIGURES

1   SUMMARY

Ground-based radiometric techniques were applied to measure the slant path attenuation cumulative distribution function to over 20 dB of attenuation and to less than 1% exceedance probability at the V and W band frequencies of 72.5 and 82.5 GHz. These are the first such measurements in these frequency bands. Brightness temperature measurements were collected at an elevation angle of 36° in Rome NY using a four-channel radiometer that included 23.8 and 31.4 GHz receivers. A model based approach was used to invert brightness temperature to attenuation.   An atmospheric model relevant to the geographic location and statistically representative of the attenuating conditions was developed for this purpose. The main assumption of the atmospheric model was that the sources of attenuation for exceedance probabilities of concern were dominated by stratiform rain.   Monte-Carlo solutions to the radiative transfer equation for the precipitating atmosphere were used to generate the attenuation retrieval algorithm.   Sensitivity analysis showed that the attenuation retrieval algorithm was robust to uncertainties in the model parameters. Slant path attenuation was also measured with the radiometer using the sun as a source of radiation. Over 30 dB of attenuation dynamic range was possible with this technique.   Sun-beacon measurements were used to test model predictions.

2 INTRODUCTION

The V/W satellite communication bands of 71-76 GHz downlink and 81-86 GHz uplink are attractive due to the available spectrum and large bandwidth. Reliable attenuation prediction capabilities are needed in order to analyze the utility and design requirements of a V/W satellite communications system. Extrapolation of existing models based on low frequency attenuation statistics has significant uncertainty [Brost et al., 2011; Brost 2012]. There have not been any slant path attenuation statistics measurements made at the V and W bands with which to validate or develop attenuation prediction models. The type of data needed is attenuation measurements made on a continuous basis for time periods in one year increments and temporal resolution better than 10 s. Radiometers offer the possibility to obtain the much needed attenuation statistics, albeit with certain limitations. Under the assumption of local thermodynamic equilibrium (LTE) the brightness temperature T_b measured by a radiometer can be related to the atmosphere it is sensing through radiative transfer theory [Chandrasekhar, 1960; Brussaard, 1984]. A scalar form of the radiative transfer equation (RTE) is given by [Ulaby et al., 1981],

$$T_b(r) = T_0 e^{-\tau(0,r)} + \int_0^r k_e(r') \left[(1-a)T(r') + aT_{SC}(r')\right]e^{-\tau(r,r')}dr' \tag{1}$$

where $T_b(r)$ is the brightness temperature at the receiving antenna resulting from the contribution of the medium up to a distance r, $T(r')$ is the physical temperature at level r', T_0 is the brightness temperature at the boundary, T_{SC} is the average scattered radiation temperature, k_e is the

extinction coefficient, k_s is the scattering coefficient, a is the scattering albedo k_s/k_e, and τ is the optical thickness defined as

$$\tau(r,r') = \int_r^{r'} k_e(s)ds \ . \tag{2}$$

The terms in equations (1) and (2) pertain to propagation in the direction **r**. For an up-looking radiometer T_0 is the cosmic background temperature (2.73 K), and

$$\tau = \tau(0,\infty) = \int_0^\infty k_e(r')dr' \tag{3}$$

is the opacity, or total atmospheric attenuation. The formulation for scattering atmospheres is indeed more complicated than implied by equation (1). This is because the scattered radiometric temperature T_{SC} at every point is determined by an integral involving the radiation received in all directions over a 4π solid angle and the scattering phase function at that point. The task of applying radiometry is to relate T_b to τ. By defining the effective medium temperature

$$T_{mr} = \frac{T_b - T_0 e^{-\tau\prime}}{1 - e^{-\tau}} \tag{4}$$

the path attenuation A in decibels can be expressed as

$$A = 10\log_{10}\left(\frac{T_{mr} - 2.73}{T_{mr} - T_b}\right) \ . \tag{5}$$

T_{mr} corresponds to the temperature of a uniform absorptive atmosphere with attenuation A that would produce a brightness temperature T_b. For atmospheres with attenuation less than about 10 dB an approximate value of T_{mr} is often sufficient to provide an acceptable estimate of the attenuation [Allnutt et al., 1994; Brussard, 1984; Shimabukuro et al. 1984]. This was confirmed experimentally as attenuation data derived from radiometer measurements at 20 and 30 GHz

were shown to match well with beacon attenuation measurements to over 10 dB [Allnutt et al., 1994].

Estimates of T_{mr} can be determined from the surface meteorological data [Liljegren et al., 2001; Liou, 2000]. At higher attenuation levels T_b becomes sensitive to the details of the attenuation and temperature profiles and the use of equation (1) requires accurate estimates of T_{mr} due to the nonlinear behavior of equation (5) when T_b is close to T_{mr}. The usual estimates of T_{mr} based on radiosonde and climatic data are no longer reliable under these conditions. The problem is that T_{mr} is a function of the unknown atmosphere that is being sensed and can be quite different than the climatic average. With brightness temperature resolution better than 0.2 K it is possible to differentiate atmospheric attenuation to levels greater than 20 dB. However there is no generalized formulation for inverting equation (1) to retrieve these higher levels of attenuation, and consequently there has been little use of radiometers in this regime.

A variety of measurements of atmospheric emissions at V and W band frequencies have been made with ground-based radiometers [Wrixon, 1971; Davies, 1975; Westwater et al., 1990; Mätzler, 1992; Sheppard, 1996]. But none of these studies provided the needed statistics. The measurements of Westwater et al. [1990]; Mätzler [1992]; and Davies et al. [1998] were limited to clear and cloudy conditions. Sheppard [1996] examined the effect of liquid precipitation on the retrieval of integrated water vapor and liquid water path. Wrixon [1971] and Davies [1975] used sun-tracking techniques to measure 90 GHz and 71 GHz attenuation respectively. The measurements of Davies [1975] were limited in dynamic range and the measurements were for only a six month period. The main difficulty with sun-tracking experiments is that it is problematic to determine the appropriate attenuation and meteorological statistics needed for prediction models.

The downwelling brightness temperature measured in a rainy atmosphere is generally somewhat less than would be measured in a purely absorptive atmosphere with the same attenuation, due to scattering by the rain drops. This led some researchers to conclude that apparent attenuation determined by equation (5) would under-estimate the true attenuation [Zavody, 1974; Ishimaru and Cheung, 1980; Shimabukuro et al., 1984]. This conclusion was based on the assumption that the T_{mr} being used was correct for an absorbing atmosphere. In practice the estimated T_{mr} is different than this. The apparent attenuation can be either greater or less than the true attenuation. In our case, we have found that using the climatic T_{mr} in equation (5) over-estimated attenuation at the higher attenuation levels.

A way to improve attenuation retrieval dynamic range and accuracy is with a model based approach in which the RTE is used to calculate radiometer brightness temperature for representative model atmospheres. The efficacy of this approach was demonstrated by Hornbostel et al. [1994] and Marzano [2007] who compared their predictions with beacon data. Hornbostel et al. [1994] extracted a relationship for T_{mr} as a function of brightness temperature from simulations for a plane parallel rain atmosphere and a vertical linear temperature profile. The radiometer based attenuation statistics fitted the 20 GHz beacon attenuation statistics to 25 dB with a maximum relative error of 4%.   Marzano [2007] developed a model based method to predict brightness temperature due rainfall along slant paths. The approach was based on multiple regression analysis trained by a 5000 cloud radiative data set derived from a cloud mesoscale model. The atmospheric cloud model assumed planar stratified medium with seven homogeneous layers of hydrometeors. Comparison with beacon attenuation and radiometric data showed fairly good agreement.

In this in-house final report we discuss the use of radiometric techniques to determine V and W band slant-path attenuation cumulative distribution functions (CDFs) at 72.5 and 82.5 GHz. Section 2 describes the experimental details of the slant path measurements. We employed a model-based approach to retrieve attenuation to over 20 dB from the measured brightness temperatures. The modeling methodology and sensitivity analysis to model assumptions and parameters are described in section 3. Results and analysis of the data are given in section 4. We also directly measured the slant-path attenuation with the radiometer in a Sun-beacon mode which can directly measure attenuation with a dynamic range greater than 30 dB.

3 METHODS, ASSUMPTIONS, AND PROCEDURES

3.1 Slant-Path

Radiometric data was collected in Rome, NY (43.2° N, 75.4°W). The radiometer used in our experiments was a four channel liquid water profiler with receivers at 23.8, 31.4, 72.5 and 82.5 GHz. The four channels of the RPG model LWP-U72-U82 radiometer share a common parabolic antenna of 30 cm diameter. The antenna is protected by a radome and has a heated blower to mitigate affects due to hydrometeors. Brightness temperature resolution of the radiometer is better than 0.2 K at the 1 second integration time used in the data collection. The antenna gain characteristics were measured by scanning the radiometer across the sun. The measured brightness temperature is a convolution of the gain profile with the Sun. For the beamwidths of this radiometer the convolution is nearly the same as the antenna gain profile. The gain profiles could be described as Gaussian shaped with FWHM beamwidths of 3.74, 2.97, 1.47 and 1.30 degrees for the 23.8, 31.4, 72.5 and 82.5 GHz channels respectively.

Brightness temperatures were measured at an elevation angle of 36° on a continuous basis except for minor outages due to power failures and calibrations. The 36° elevation angle is representative of conditions that might be utilized for a V/W satellite communications system. We report on slant path measurements that were collected for the one year period of 1 Feb 2011 to 31 Jan 2012. The Ka-band receivers at frequencies of 23.8 and 31.4 GHz allow measurement of the cloud liquid water path (LWP) and the integrated water vapor (IWV). The slant path statistics for this time period were close to the International Telecommunication Union (ITU) model predictions for this location [ITU-R, 2013; ITU-R, 2009].

3.2 Sun-Beacon

A radiometric technique that directly measures slant path attenuation uses the sun as a source of radiation [Hogg and Chu, 1975]. The sun can be modeled as a uniform disk of 32 minutes of arc for frequencies greater than 10 GHz [Croom, 1968]. A slowly varying component is maximum at frequencies of about 2-5 GHz, and is generally not detectable at frequencies above 25 GHz [Croom, 1968]. The brightness temperature of a radiometer pointing at the sun is given by

$$T_b = T_A + T_S e^{-\tau} \quad , \tag{6}$$

where T_A is the brightness temperature due to the atmosphere, τ is the opacity of the atmosphere, and T_S is the contribution from the sun in the absence of any atmospheric attenuation. In this technique the knowledge of the solar strength is not required, only the magnitude of T_S is needed. T_S depends on frequency and beamwidth and can be determined from measurements taken in clear weather where the opacity can be determined with good accuracy. The magnitude of T_S was 583.9 K at 72.5 GHz and 728.7 K at 82.5 GHz with a standard deviation less than 2%.

This is much less than the Sun temperature at these frequencies (6000 to 7000 K). In the switching experiment two measurements are made; one measurement pointing at the center of the sun, the other pointing off the sun. The difference is $T_S e^{-\tau}$. The pointing resolution of the radiometer was 0.1° in azimuth and elevation. The error in pointing accuracy resulted in less than 0.1dB error in attenuation. Over 30 dB of dynamic range in path attenuation measurement was possible at V and W bands with this technique. The major source of error in this technique is the assumption that the atmospheric conditions are the same along the sun and offset paths. An example of attenuation measurements made during a rain event is shown in Figure 1. These measurements were made at elevation angles between 30° and 36°. The surface temperature was approximately 12.5° C.

3.3 Modeling the Radiometric Brightness Temperature

The main goal of this effort was to provide an experimentally determined attenuation CDF at the V and W bands with a dynamic range greater than 20 dB. The approach to retrieve attenuation was to relate the V and W band attenuation to the available measured observables of radiometer brightness temperature and surface temperature (T_S), pressure (P_S) and relative humidity (RH_S). Attenuation derived from equation (5) with a T_{mr} that was a function of T_S, P_S, and RH_S was assumed valid for $A < 10$ dB. For higher levels of attenuation a model-based retrieval algorithm was applied. The methodology was to apply a statistically representative model of the atmospheric conditions and calculate the vector $A(T_b,T_S,P_S,RH_S,R)$ that related the attenuation to the measured observables and an atmosphere that was parameterized by the rain rate R. The main assumption guiding the radiometric modeling was that the 72.5 and 82.5 GHz slant-path attenuation statistics could be satisfactorily determined with an attenuation model that was descriptive of widespread stratiform rain corresponding to the rain with bright band model

number 2 of Fabry and Zawadzki [1995]. With the high rain specific attenuation at these frequencies attenuation levels could exceed 20 dB with rainfall rates of only a few mm/hr at the 36° elevation angle used. The underlying assumption was that the attenuation statistics at these levels were dominated by stratiform rain and that retrieval errors associated with convective rain would have little impact on the statistics.

3.4 Background Atmosphere

A parametric atmospheric model was developed for this location that described the altitude dependence of temperature, pressure, and water vapor as a function of the surface temperature, pressure, and relative humidity, based on radiosonde data (Albany, NY) and numerical weather models.   The altitude dependence of pressure and water vapor concentration were modeled as

$$P(h) = P_S e^{-\frac{h}{7.5}} \tag{7}$$

$$\rho(h) = \rho_S e^{-\frac{h}{2.5}} \tag{8}$$

where h is in km. The temperature profile and freezing level are important parameters for radiometric modeling of rainy atmospheres. We developed two models for temperature profiles. The first model determined the altitude dependence of atmospheric temperature from the surface meteorological conditions consistent with a model for the freezing level as a function of surface temperature. The second model allowed the freezing level to be specified and the temperature profile was matched to this. The average freezing level increased approximately linearly with surface temperature with an average height of about 3.3 km for the months of May to October. Freezing level variability is quite significant with a standard deviation of approximately 400 to 800 m, depending on surface temperature.

3.5 Rain

The attenuating atmospheric model was comprised of a stratiform rain model that was imposed on the background atmosphere. The model, which included a melting layer and clouds, was parameterized by the surface meteorological conditions and the rain rate. The rain field was assumed to be uniform in the horizontal plane and the rain height determined by the freezing level. Rain drop size distributions (DSD) were assumed to be described by the gamma distribution:

$$N(D) = N_0 D^\nu e^{-\Lambda D}, \tag{9}$$

where *N(D)* is the differential number density and D is the rain drop diameter. The coefficient N_0 and slope parameter Λ may be functions of the rain rate. The Marshall and Palmer (MP) DSD [Marshall and Palmer, 1948] is commonly considered appropriate for stratiform rain [Olsen et al., 1980; Sauvageot, 1992]. We used this DSD for our rain and melting layer models. Given the variability in rain drop size distributions, we also examined the Laws and Parsons (LP) [Laws and Parsons 1943] and the Joss-Thunderstorm (JT) [Joss et al., 1968] DSDs to determine the sensitivity to this parameter. As polarization effects were not considered the extinction and scattering parameters for the rain were determined from Mie scattering theory. Scattering albedos for rain at V and W band frequencies are approximately 0.3 to 0.5 for the rain DSDs and rain rates considered. The temperature of rain was taken to be the wet bulb temperature. We assumed the atmospheric relative humidity to be 90%, which resulted in a rain temperature about 1K below the atmospheric temperature.

3.6 Melting Layer

A melting layer radiative model was derived from analysis based on commonly used melting layer model formulations which assumed spherical melting particles with no coalescence or breakup [Yokomata and Tanaka, 1984; Szyrmer and Zawadzki, 1999; Bataglia et al., 2003]. The microphysical and electromagnetic properties of the melting layer can be determined from the rainfall rate and rain DSD subject to the parameterizations of snow density, particle velocities, ventilation coefficient, dielectric model, and dielectric mixing rule. Model parameters have typically been selected by matching the model to reflectivity data. A variety of parameterizations have been possible. Therefore, a definitive melting layer model has not been established with which to determine V and W band radiative properties. Furthermore, extinction and scattering characteristics are not assured from parameterizations derived from matching to reflectivity data. Indeed, we have observed that some parameterizations that gave similar reflectivity characteristics produced significantly different radiative characteristics. The melting layer model implemented in this study reflected the general behavior observed from the melting layer analysis, but with some uncertainty in magnitude. The melting layer was assumed to be a uniform layer extending to 400 m below the 0° isotherm. The averaged extinction coefficient increased with rain rate relative to the rain extinction coefficient with a magnitude that depended on rain DSD, as shown in Figure 2. The predicted scattering albedo either increased or decreased, depending on the dielectric model. We set the melting layer scattering albedo to that of the rain. The asymmetry parameter did not have a significant dependence on the dielectric model. The average change in asymmetry parameter was an increase by about a factor of 3.

3.7 Cloud Snow

The snow region above the melting layer is a potential source of attenuation for the V and W bands and was included in the rain attenuation model. This a region of about 1 to 2 km in which the ice particles aggregate to form large irregularly shaped snowflakes. The melting layer model assumption of constant mass flux means that the liquid equivalent snow fall rate at the top of the melting layer should be the same as the rainfall rate. To model the radiative characteristics of the snow cloud we have assumed that the average snow extinction was related to the rain rate by a power law relation

$$ks_e = \alpha R^\beta \quad (\text{km}^{-1}), \tag{10}$$

where $\beta \approx 1$ and α is a frequency dependent parameter. Determination of α is uncertain as there is little experimental data and theoretical values depend on model assumptions. The measurements of snow cloud attenuation by Li et al. [2001] and the analysis by Heymsfield et al. [2007] both indicated a specific attenuation of about 0.2 dB/km at 94 GHz for a rain rate of about 4 mm/hr. We took $\alpha = 0.012$ (hr/m^2) and $\beta = 1$ at 94 GHz and scaled to other frequencies resulting in a value for α of 0.007 at 72.5 GHz and .009 at 82.5 GHz. Terrestrial measurements of snow attenuation [Wallace, 1984; Nemarich, 1982] suggest a somewhat greater attenuation. The scattering albedo was taken to be 0.92 and the asymmetry parameter was taken to be 0.6. The snow layer depth was set at 1.5 km.

3.8 Cloud Water

The zenith cloud liquid water path was determined from rain height and rain rate through the relation proposed by Wentz and Spencer [1998].

$$LWP = .18\left(1 + \sqrt{H_R R}\right) \tag{11}$$

Here LWP is in kg/m^2 when H_R is in km and R is in mm/hr. A uniform cloud extending 1.5 km below the zero degree isotherm was assumed. This model resulted cloud liquid water content generally less than 1 gm^{-3} and in attenuations up to a few dB. The LWP determined by equation (11) was mapped onto the measured rain rate cumulative distribution function (CDF) with an average rain height of 3.3 km and compared with the cloud LWP CDF predicted by the ITU-R. P840 model. The calculated LWP was about one half of that predicted by the ITU cloud model for the same time percentages. This indicates that the cloud model is statistically representative, although the correlation with rain is an assumption.

3.9 Radiative Transfer Model

The radiometer brightness temperature was calculated for different conditions within the framework of this atmospheric model. The rain and ice scattering albedos at 72.5 and 82.5 GHz are significant and it was necessary to use a radiative transfer model that accounted for scattering.   A Monte Carlo simulation which allowed three dimensional photon trajectories was used to solve the radiative transfer for scattering atmospheres. The approach was similar to that described by Mayer [2009] and Roberti et al., [1994].   Photons were launched from the radiometer and traced backwards to their source of emission. The scattering phase function was

determined from the asymmetry parameter g. If g was greater or equal to 0.2 the phase function was approximated by the Henyey–Greenstein phase function [Henyey and Greenstein, 1941]. Here the cosine of the scattering angle was given by

$$\mu = \frac{1}{2g}\left[1 + g^2 - \left(\frac{g^2-1}{2gr-g-1}\right)^2\right] \quad , \tag{12}$$

where r is a random number between 0 and 1. For smaller asymmetry parameters the Henyey – Greenstein phase function under-estimates scattering in the backwards direction. If g was less than 0.2 a combined Henyey-Greenstein and Rayleigh phase function proposed by Liu and Weng [2006] was used. Here the phase function is given by

$$P(\mu, G(g)) = C\frac{3}{8}(1 + \mu^2)\frac{1}{2}\frac{1-G^2}{[1+G^2-2G\mu]^{3/2}} \tag{13}$$

where C is a normalization constant and G is function of g and is approximately equal to g. Its expression is given in Liu and Weng [2006]. The scattering angle was determined by a random draw from the phase function CDF. The ground was assumed to be at the same temperature as the surface temperature with an emissivity of 0.95 and Lambertian phase function.

3.10 Sensitivity Analysis

A sensitivity analysis examined the impact of various parameters on the relationship between attenuation and brightness temperature. Figure 3 shows some representative results for 72.5 GHz. With the predominant forward scattering, brightness temperature is generally less than a purely absorbing atmosphere with the same attenuation coefficient. This is seen in Figure 3a which compares the calculated radiometric response at 72.5 GHz for different rain DSDs; the Marshall-Palmer (MP), Laws-Parsons (LP), and Joss Thunderstorm (JT). Also shown is the

calculated brightness temperature for MP DSD with the scattering albedo set to zero. Although attenuation and brightness temperature depended on rain height for a given rain rate, the rain height only weakly affected the attenuation-brightness temperature curves (Figure 3b). This can be understood by considering that the rain rate and temperature profile both change such that the temperature of the mean photon path length is approximately constant. Similarly, the attenuation–brightness temperature characteristics were not changed much by modest variations (factors of up to 2 or 3) in the relevant parameters for the melting layer and cloud. The greatest sensitivity was found to be the dependence on surface temperature. Figure 4 shows the 72.5 GHz attenuation as a function of brightness temperature for different surface temperatures.

3.11 Attenuation Retrieval Algorithm.

The results of the sensitivity analysis showed that the attenuation-brightness temperature characteristics were quite robust to most of the model parameters. Consequently an attenuation retrieval algorithm could be achieved by relating the attenuation to brightness temperature and surface temperature for the modeled rain and cloud parameterizations. The measured surface relative humidity was not used as an input parameter as the model assumed atmospheric relative humidity of 90%, which was also the average relative humidity measured for rain times. The algorithm was implemented by calculating the three-dimensional matrix of A, T_b and T_S. The attenuation was retrieved by linear interpolation with the measured values of T_b and T_S.

4 RESULTS AND DISCUSSION

4.1 Slant Path Statistics

The attenuation retrieval algorithm was applied to the measured slant path data for the four radiometer frequencies. The slant path attenuation statistics are shown in Figure 5. For the Ka band frequencies only attenuation determined from equation (5) are shown.

4.2 Algorithm–Sun Beacon Comparison

A test of the attenuation retrieval algorithm was possible by comparing the attenuation predictions with the sun-beacon data. This is shown in Figure 10 for the 72.5 GHz data for the MP and LP rain DSDs. The mean deviation was slightly less with the LP and JT DSDs compared to the MP DSD. Since the sun-beacon data is a dynamic measurement and the attenuation algorithm is a statistical model, a more appropriate test would be to average data and model deviations over many data sets. We have not collected a sufficient amount of sun-beacon data with which to make that comparison at this time.

4.3 Finite Cell Size

The attenuation retrieval model assumed that neglecting the occurrence of finite rain cells had little impact on the retrieved attenuation statistics for the relevant time percentages. To quantitatively test the validity of this assumption we compared the A-T_B calculated for a slant path (36° elevation angle) between a model of wide-spread rain and a rain cell model that included rain cell size characteristics. The concept was to estimate the statistical occurrence of convective rain cells in the radiometric data by relating their occurrence to the measured rain rate statistics. For this analysis it was convenient to assume uniform cylindrical (or square) rain cells

imbedded in large area of stratiform rain. The top-hat model was adopted from that of Misme and Waldtuffle [1980] in which the rain rate in the plateau region was related to the cell rain rate by

$$R_p = 10[1 - e^{-0.0105R}] \text{ (mm/hr)} \tag{14}$$

The utility of using a uniform rain cell model is that it provided an analytical expression for the spatial kernel associated with a given rain attenuation and rain rate, and the spatial probability of rain was easily determined from the rain rate CDF. The measured rain rate statistics were used to calculate the rain rate CDF for a specified exceedance attenuation A, rain height H_R, and rain cell diameter $D(R)$. This CDF represented the distribution of rain rates that could produce an attenuation that exceeded A. The brightness temperature and attenuation for rain rates drawn from the CDF were calculated with the three-dimensional Monte Carlo radiative transfer simulation. Attenuation from clouds and melting layer were not included in this analysis. The spatial location of the rain cell center was determined by random draw from the corresponding spatial area determined by A, H_R, $D(R)$. Different models that related rain cell size to rain rate were examined. An example calculation is shown in Figure 6 for a rain cell model given by

$$Dia(R) = 27R^{-.54} \quad \text{(km)} \tag{15}$$

and 12° C surface temperature. Scatter in the data points increased with surface temperature and depended also on the particular rain cell size model. The main conclusion of this analysis was that the uniform/ widespread rain model was most likely to under-estimate the attenuation by up to a few percent.

4.4 Cloud Attenuation

The attenuation retrieval algorithm used above was based on the assumption that attenuation above 10 dB modeled as widespread rain could provide acceptable attenuation statistics. This neglected the other category of attenuation that could be significant, that being non-precipitating clouds. We did not have a robust means to distinguish between slant-path attenuation due to clouds only and that due to a rain event. To examine the impact of cloud attenuation we calculated the attenuation-brightness temperature relationship for different cloud models that varied in altitude and size. Some results are shown in Figure 12 for two different surface temperatures. Cloud model-1 has the cloud 1km in thickness and centered at the zero degree isotherm. Model-2 has the cloud 1 km thick and the top at the zero degree isotherm. Model-3 has the cloud 2 km thick and located below the zero degree isotherm. The rain attenuation model is also shown. The result of the analysis indicated that the rain model attenuation retrieval worked well to about 15 dB, and to about 20 dB for temperatures below 12 C. The error associated with significant cloud attenuation would be to underestimate the attenuation.

The overall impact on attenuation statistics may not be very significant. At 72.5 GHz a LWP of about 4 kg/m^2 would be needed to exceed 15 dB of attenuation. Extension of the cloud statistics in line with the ITU model would imply that such high cloud attenuation should occur less than 0.1% of the time, especially when considering that the ITU model is for both precipitating and non-precipitating clouds. We conclude that the attenuation statistics are only negligibly affected by inaccuracies associated with non-precipitating clouds

4.5 Rain DSD

The choice of rain drop size distribution was found to have little impact on the slant path statistics as shown in Figure 9.

4.6 Surface Temperature

The attenuation retrieval algorithm was most sensitive to surface temperature. This sensitivity is shown in Figure 10 where we the attenuation exceedances for 72.5 GHz with the surface temperature adjusted by +/- 1K. This is an uncertainty in attenuation retrieval of about 1dB/K at 20 dB of attenuation. An uncertainty in the surface temperature can arise, not from the temperature sensor, but rather due to variations in temperature on the slant path. Our retrieval relied on a point temperature measurement, not a path averaged measurement.

4.7 K-band Frequencies

We considered the use of the K-band frequencies in the attenuation retrieval. It was found it to be of limited value. Although the V and W band attenuation-brightness temperature characteristics did not depend strongly on the model parameters, the V and W band attenuation relationships to the K-band brightness temperatures and attenuations were much more sensitive to model assumptions. This is because there is no unique scaling from K-band attenuation to V or W band attenuation. It very much depends on the source of attenuation and rain DSD. Another application of the K-band measurements that we considered was the identification of erroneous V/W band attenuation retrievals, such as might result from finite rain cell size or non-precipitating clouds as discussed above. If the K-band attenuation were high, then it could be assumed that the V and W band attenuations should also be high with some minimum scaling

ratio.   We examined a range of K-band attenuation thresholds and scaling ratios.   While we could identify some questionable V/W band attenuation retrievals, the impact on the attenuation statistics was negligible.

5   CONCLUSION

Ground-based radiometric techniques were applied to measure the slant path attenuation cumulative distribution function at the V and W band frequencies of 72.5 and 82.5 GHz. These are the first slant-path measurements in these frequency bands. A model based approach was used to invert brightness temperature to over 20 dB of attenuation.   An atmospheric model relevant to the geographic location and statistically representative of the attenuating conditions was developed for this purpose. The main assumption of the atmospheric model was that the sources of attenuation for exceedance probabilities of concern were dominated by stratiform rain. Monte-Carlo solutions to the radiative transfer equation for the precipitating atmosphere were used to generate the attenuation retrieval algorithm. Sensitivity analysis showed that within the context of this atmospheric model, attenuation retrieval was robust to uncertainties in the parameterizations of the rain height, melting layer, cloud content, and rain drop size distribution. This allowed for an attenuation retrieval that depended only on surface temperature and brightness temperature. Consequently, the use of a single point measurement of surface temperature introduced some uncertainty in the attenuation retrieval.   Slant path attenuation was also measured with the radiometer using the sun as a source of radiation. Over 30 dB of attenuation dynamic range was possible with this technique. Sun-beacon measurements were used to test model predictions.

Acknowledgements

Brightness temperature data for this paper are available by contacting the authors.

6 REFERENCES

Allnutt R., Pratt T., Stutzman W., and Snider J. (1994), "Use of radiometers in atmospheric attenuation measurments", *IEE Proc. Microw. Antennnas Propag*., vol. 141, 428-432.

Battaglia, A., C. Kummerow, D. Shin, and C. Williams (2003), Constraining microwave brightness temperatures by radar brightband observations,*J. Atmos. Oceanic Technol.*, *20*, 856 – 871.

Brost, G. (2012) , "Influence of the rain cell structure on attenuation predictions on earth-space paths," Antennas and Propagation (EUCAP), 2012, 6th European Conference on , vol., no., pp.3149-3153, 26-30 March 2012 doi: 10.1109/EuCAP.2012.6205915.

Brost G., Cook W. (2012), "Analysis of empirical rain attenuation models for satellite communications at Q to W band frequencies", 6th European Conference on Antennas and Propagation (EUCAP), 2012, 10.1109/EuCAP.2012.6205935, pp. 1455-1459.

Brost G., Cook W., and Lipe W. (2011)," On the modeling and prediction of Attenuation for V/W Satellite Communications", Ka and Broadband Communications Conference, Palermo, Italy.

Brussaard G. (1984), "*Radiometry - a useful prediction tool?*", ESA SP-1071, EDA, Paris, France.

Chandrasekhar S. (1960), *Radiative Transfer*, Dover Publications, New York, 1960.

Croom D. (1973), "Sun as a broadband source for tropospheric attenuation measurements at millimetre wavelengths", *Proc. IEE*, vol 120, 1200-1206.

Davies, P.G. (1975): "Attenuation by cloud and rain on earth-sun paths at 12 to 71 GHz", *Electron. Lett*., 11, 547-548.

Davies, O.T., R.G. Howell, and P.A. Watson (1998): "Measurement and modelling of cloud attenuation at millimetre wavelengths", *Electron Lett.*, 34, 2433-2434.

Henyey L. and Greenstein J. (1941), "Diffuse radiation in the galaxy", *Astrophys. J.,* vol 93, 79-83.

Hogg, D.C. and T. Chu (1975): "The role of rain in satellite communications", *Proc. IEEE*, 63, 1308-1331.

Hornbostel A. and Schroth A. and Kutuza B. (1994),:"Polarimetric Measurements and model measurements of downwelling rain brightness temperature", *Proceedings of μrad94*, Rome, Italy.

International Telecommunication Union-Radiocommunication (ITU-R) (2009b), Water vapour: surface density and total columnar content, *Recomm ITU-R P.836-4*, Geneva, Switzerland.

International Telecommunication Union-Radiocommunication (ITU-R) (2013), Attenuation due to clouds and fog., *Recomm ITU-R P.840-6*, Geneva, Switzerland.

Ishimaru A. and Cheung R. (1980), "Multiple-scattering effect on radiometric determination of rain attenuation at millimeter wavelengths", *Radio Science*, vol 15, 507-516.

Joss, J., J.C. Thams, and A. Waldvogel (1968): "the variation of raindrop size distributions in Locarno", in *Proc. Int. Conf. Cloud Physics*, 369-373.

Laws, J.O. and D.A. Parsons (1943): "The relation of raindrop-size to intensity", *Tans. Amer. Geophys. Union*, 24, 452-460.

Liljegren J., Clothiaux E. (2001), G.G. Mace, S. Kato, and X. Dong: " A new retrieval for cloud liquid water path using a ground-based microwave radiometer and measurements of cloud temperature", *J. Geophys. Res*. vol 106, pp 14485-14500.

Li, L., S. M. Sekelsky, S. C. Reising, C.T. Swift, S. L. Durden, G. A. Sadowy, S. J. Dinardo, F.K. Li, A. Huffman, G. Stephens, D.M. Babb, and H.W. Rosenberger, (2001): "Retrieval of atmospheric attenuation using combined ground-based and airborne 95-GHz cloud radar measurements", *J. Atmos. Oceanic Technol.* , 18, 1345-1353.

Liou Y. (2000): "Radiometric observation of atmospheric influence on space-to-earth Ka-band propagation in Taiwan", *Proc. Natl. Sci. Counc*. vol 24, pp 238-247.

Liu Q. and Weng F. (2006): "Combined Henyey-Greenstein and Rayleigh phase function", *Applied Optics*, vol 45 pp7475-7479.

Marshall J. and W. Palmer , (1948):"The distribution of raindrops with size", *Journal Meteorology*, 5, 165-166.

Marzano F. (2007): "Predicting antenna noise temperature due to rain clouds at microwave and millimeter-wave frequencies," *IEEE Trans. Antennas and Propagat*., vol. 55, n. 7, pp. 2022-2031.

Mätzler, C. (1992): "Ground-based observations of atmospheric radiation at 5, 10, 21, 35, and 94 GHz", *Radio Science*, 27, 403-415.

Mayer B. (2009): "Radiative transfer in the cloudy atmosphere", *Eur. Phys. J. Conferences* 1, pp 75-99.

Misme P. and Waldteufel P. (1980): " A model for attenuation by precipitation on microwave earth-space link", *Radio Science*, vol 15 pp. 655-665.

Nemarich,J. and R. J. Wellman, and J. Lacombe, (1988): "Backscatter and attenuation by falling snow and rain at 96, 140, and 225 GHz.", *IEEE Trans. Geosci. Remote Sensing*, 26. 319-329.

Olsen, L., Rogers D., and Hodge D. (1978): " The aR^b relation in the calculation of rain attenuation", *IEEE Trans. Ant. Prop*, vol 26, pp318-329.

Roberti, L., J. Haferman, and C. Kummerow (1994): "Microwave radiative transfer through horizontally inhomogenous precipitating clouds", *J. Geophys. Res*. 99, 16707-16618.

Sauvageot H., (1992): "*Radar Meteorology*", Artech House, Boston.

Sheppard, B.E. (1996): "Effect of rain on ground-based microwave radiometric measurements in the 20-90-GHz range", *J. Atmos. Oceanic Tech*., 13, 1139-1151.

Shimabukuro F., Tavis M., and Chang D. (1984), "EHF attenuation derived from emission temperatures in light rain", *Radio Science,* vol. 19, 1535-1542.

Szyrmer, W., and I. Zawadzki (1999):Modeling of the melting layer. Part I: Dynamics and microphysics, *J. Atmos. Sci.*, *56*, 3573 – 3592.

Wallace, H.B, (1988): "Millimeter-wave propagation measurements at the Ballistic Research Laboratory", *IEEE Tans. Geos. Remote Sens.*, 26, 253-258.

Wentz F. and Spencer R. (1998), "SSM/I rain retrievals with a unified all –weather ocean algorithm", *J. Atmos. Sci*., 55, 1613-1627.

Westwater, E.R., J.B. Snider, and M.J. Falls (1990): "Ground-based radiometric observations of atmospheric emission and attenuation at 20.6, 31.65, and 90 GHz: a comparison of measurements and theory", *IEEE Trans. Ant. Prop.*, 38, 1569-1580.

Yokoyama, T., and H. Tanaka (1984): " Microphysical processes of melt- ing snowflakes detected by two-wavelength radar. Part I. Principle of measurement based on model calculation.", *J. Meteor. Soc. Japan,* **62,** 650–666.

Zavody A. (1974), "Effect of scattering by rain on radiometer measurements at millimetre wavelengths", *Proc. IEE*, vol 121, 257-263.
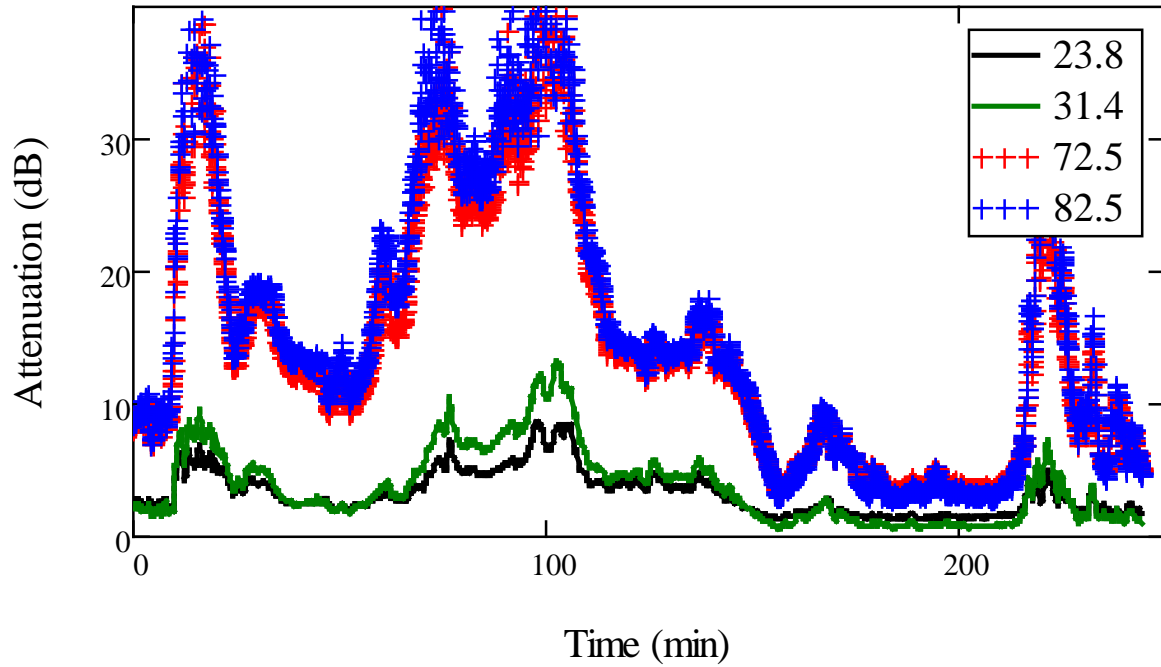
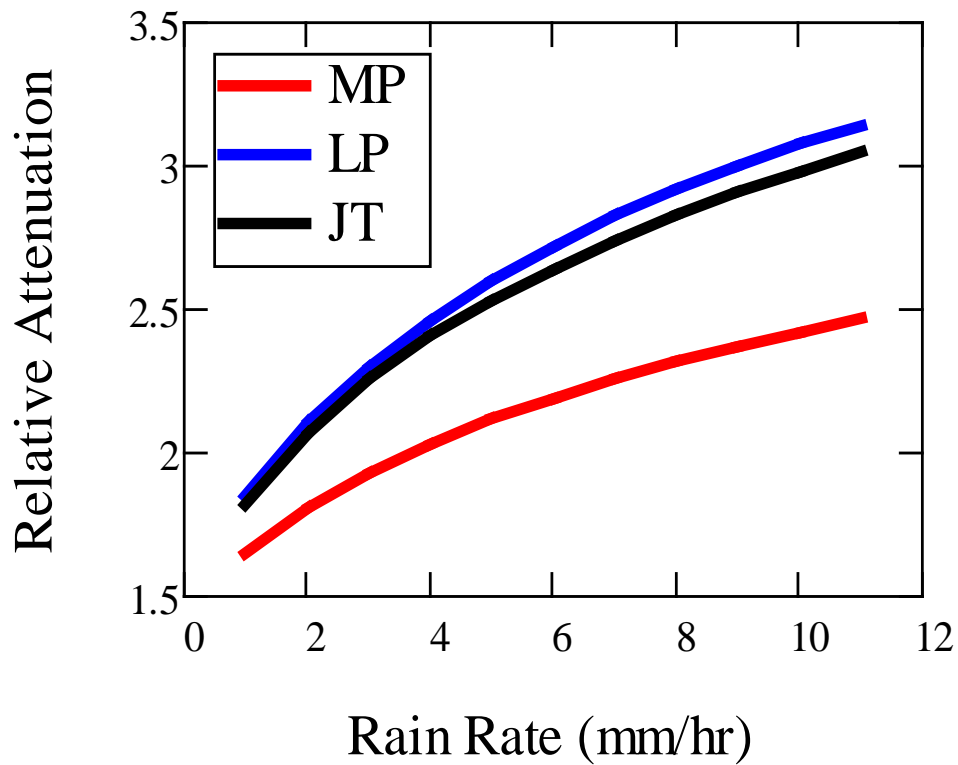Figure 1. Sun-beacon attenuation measurements during a rain event.

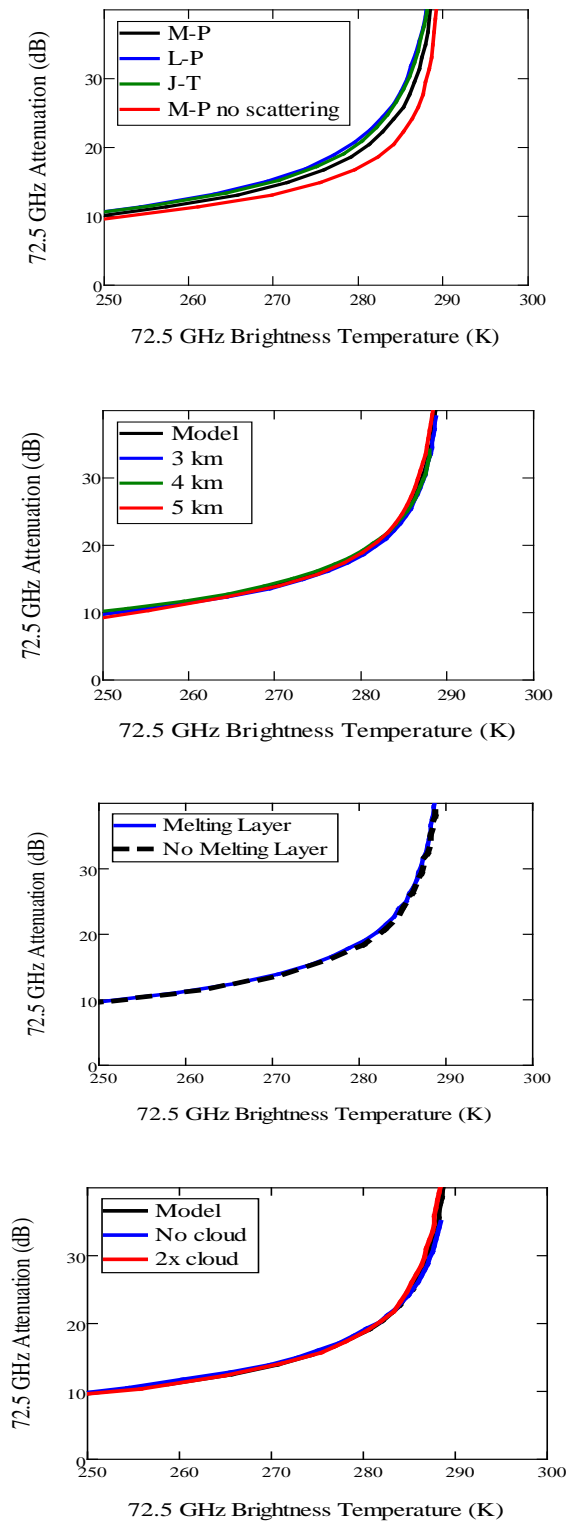Figure 2. Relative attenuation of melting layer to rain attenuation as a function of rain rate for 72.5 GHz.

Figure 3. Attenuation versus brightness temperature at 72.5 GHz for (a) different rain DSDs, (b) different rain heights, (c) melting layer, and (d) clouds.
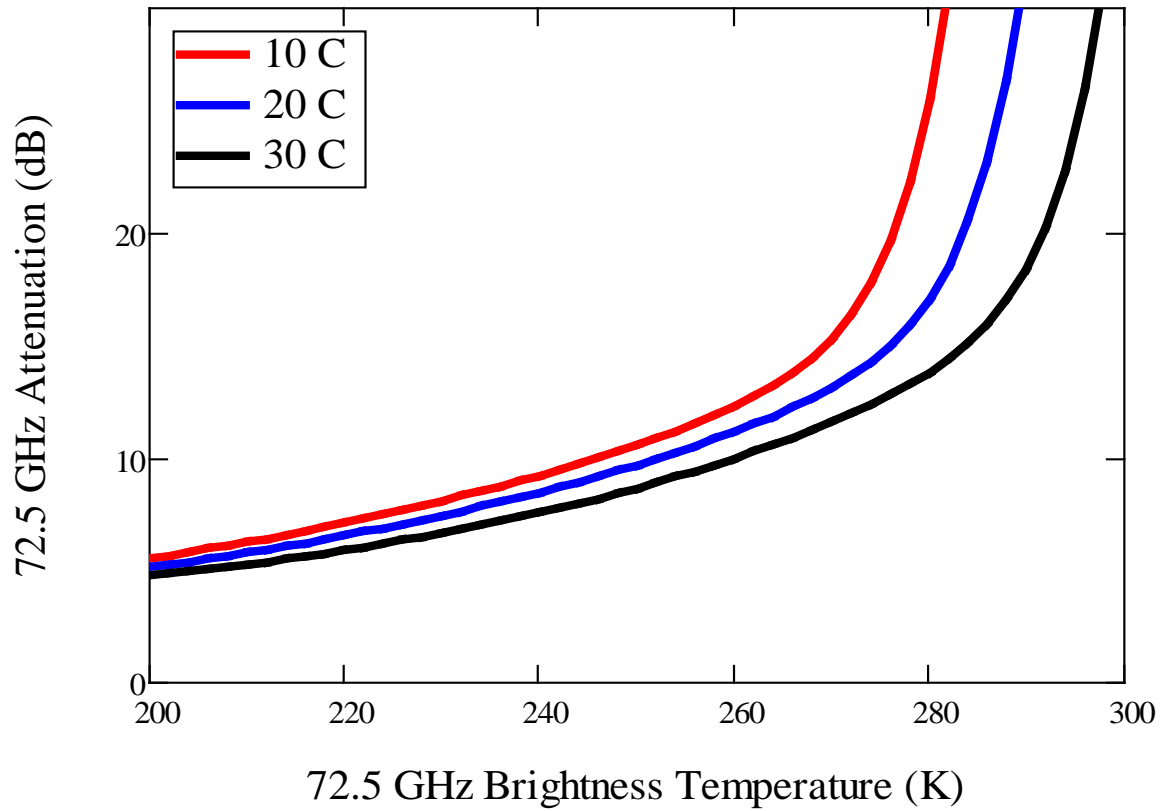
Figure 4. Attenuation versus brightness temperature for 72.5 GHz, and different surface temperatures.
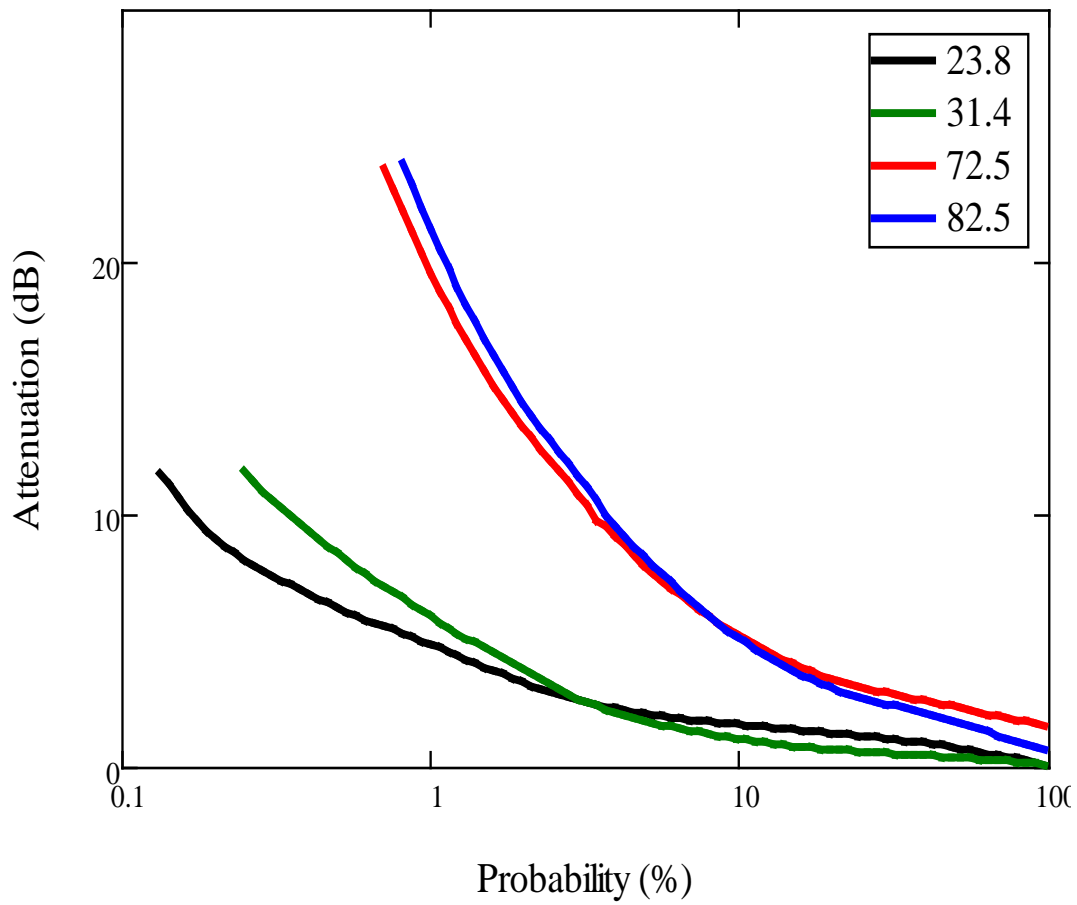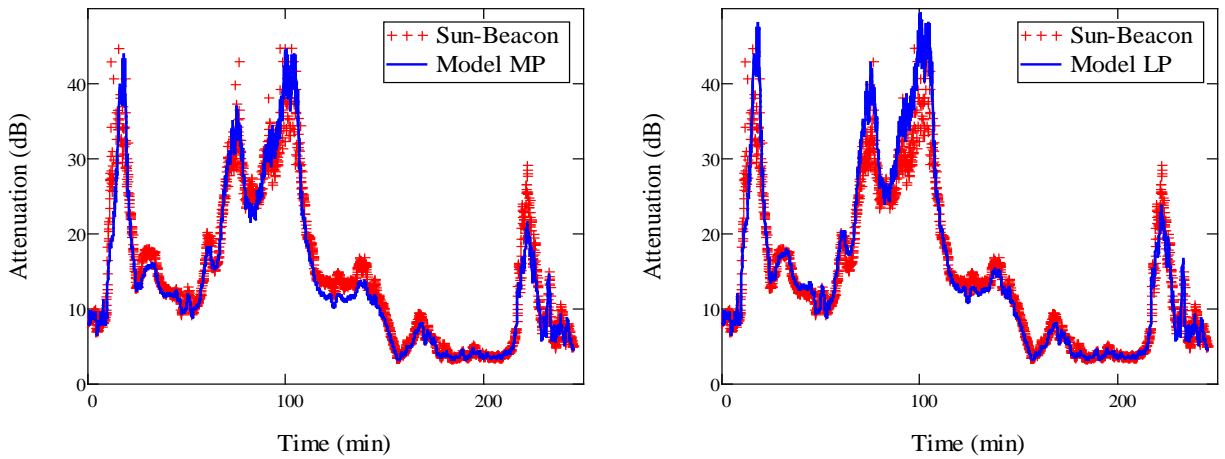
Figure 5. Attenuation statistics for Rome, NY.

Figure 6. Comparison of Sun-beacon data with attenuation retrieval algorithm at 72.5 GHz for two different rain DSDs.
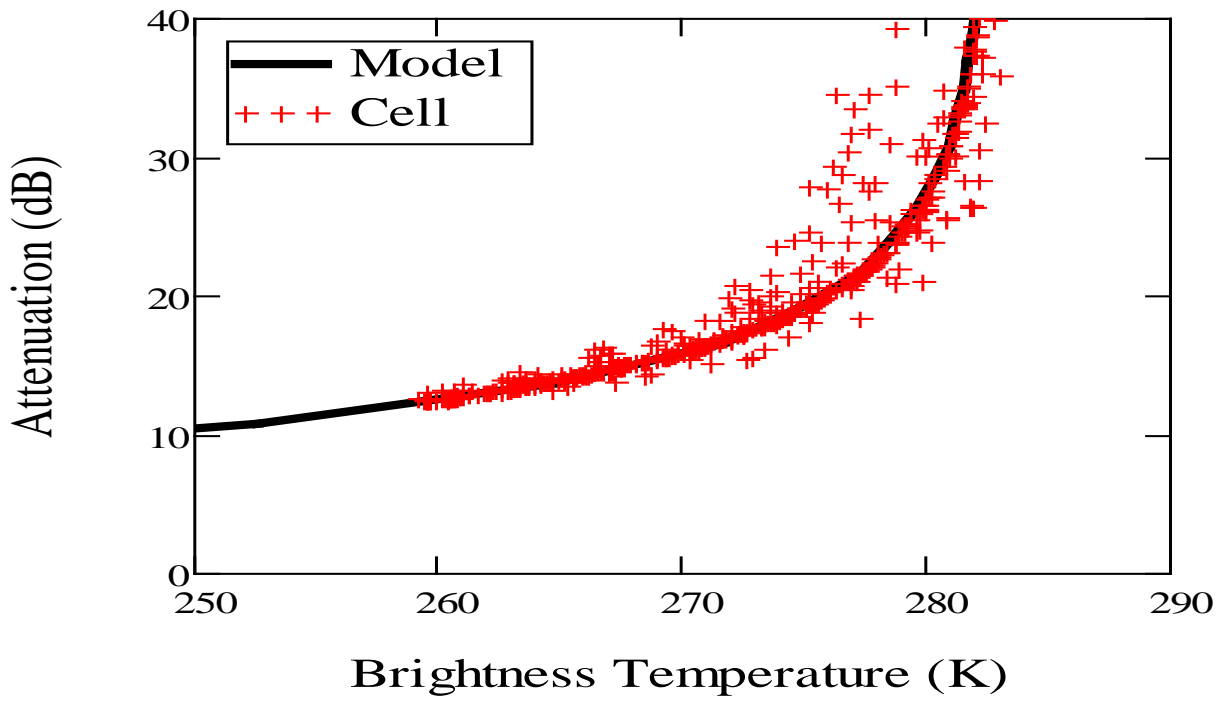
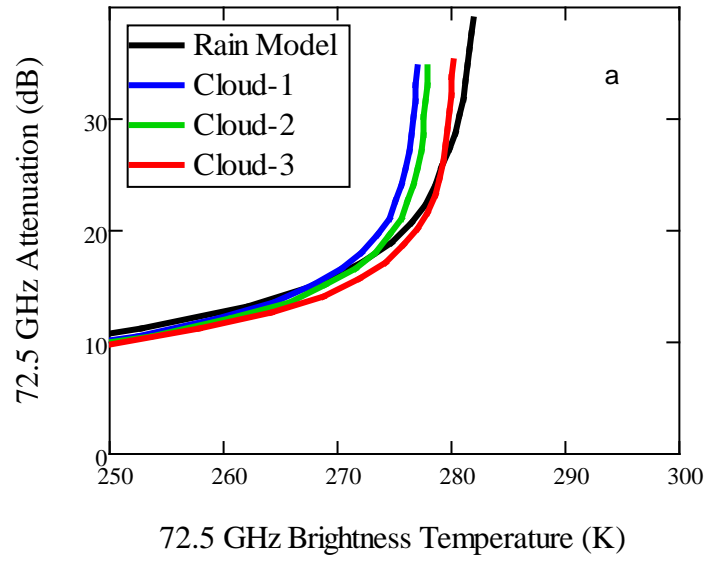Figure 7. Comparison of the uniform widespread rain model with a finite size rain cell model.
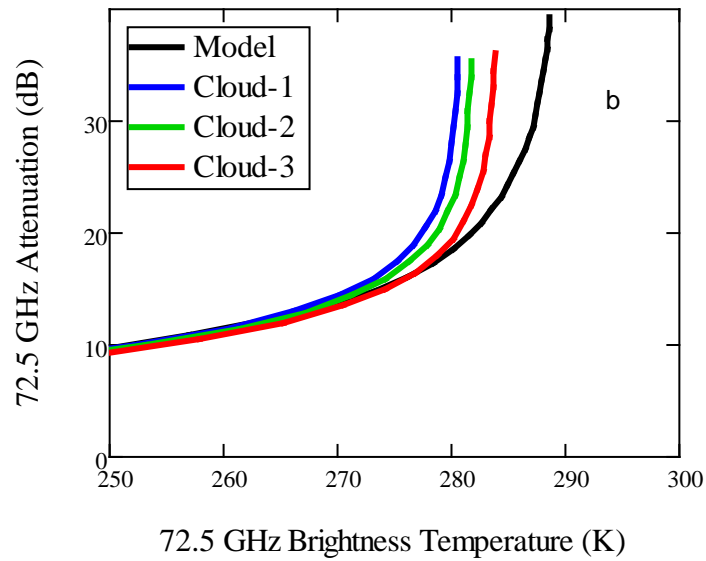
Figure 8. Attenuation versus brightness temperature for different cloud models at (a) 12°C and (b) 20°C.
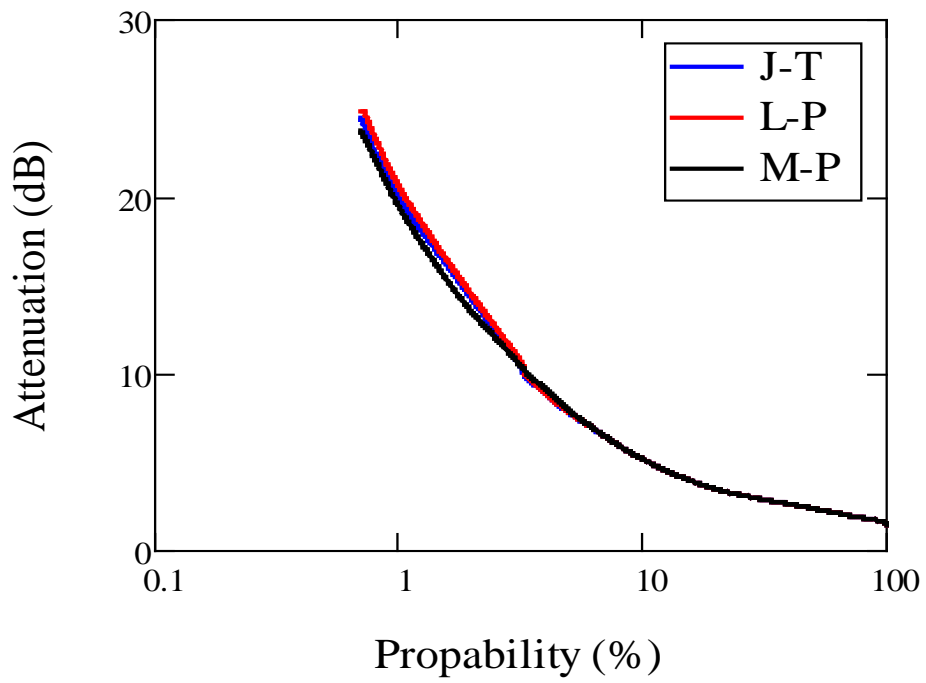
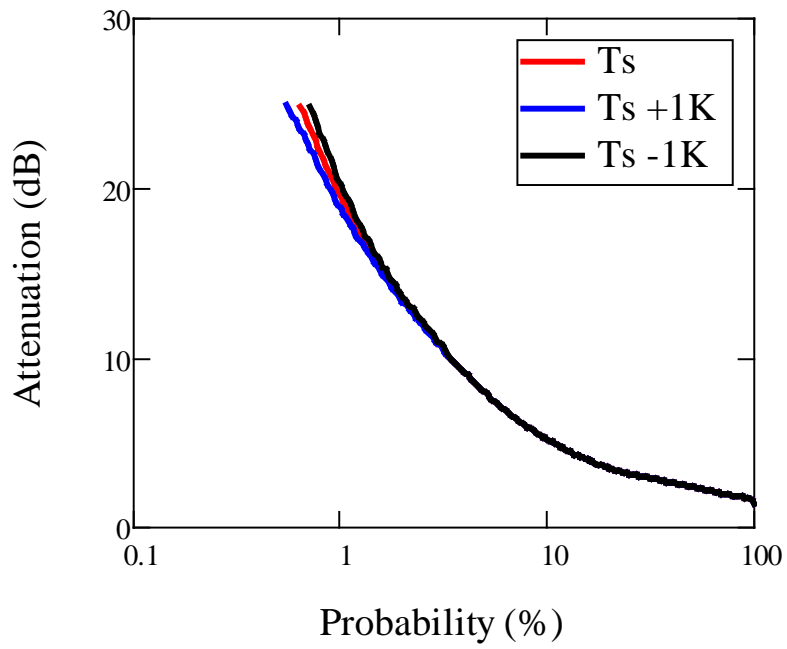Figure 9. Attenuation statistics for different rain DSDs.

Figure 10. 72.5 GHz attenuation statistics for different surface temperatures.